Supporting information

Combined experimental and computational approach to develop efficient photocatalyst based on Au/Pd-TiO$_2$ nanoparticles

Alicja Mikolajczyk[a], Anna Malankowska[b], Grzegorz Nowaczyk[c], Agnieszka Gajewicz[a], Seishiro Hirano[d], Stefan Jurga[c], Adriana Zaleska-Medynska[b], Tomasz Puzyn[a*]

[a.]   *Laboratory of Environmental Chemometrics, Faculty of Chemistry, University of Gdansk, Wita Stwosza 63, 80-308 Gdansk, Poland*
[b.]   *Department of Environmental Technology, Faculty of Chemistry, University of Gdansk, Wita Stwosza 63, 80-308 Gdansk, Poland*
[c.]   *NanoBioMedical Center, Adam Mickiewicz University, Umultowska 85, 61-614 Poznan, Poland*
[d.]   *Center for Environmental Risk Research, National Institute for Environmental Studies, Tsukuba, 16-2 Onogawa, Ibaraki 305-8506, Japan*

Corresponding Author
*E-mail: t.puzyn@qsar.eu.org
Corresponding author address: Laboratory of Environmental Chemometrics, Faculty of Chemistry, University of Gdansk, Wita Stwosza 63, 80-308 Gdansk, Poland

S1. Materials

Titanium(IV) isopropoxide (TIP) (97%), palladium(II) chloride (5 wt.% in 10 wt.% HCl) and HAuCl4 (Au≈52%)were purchased from Sigma-Aldrich. Cyclohexane, isopropyl alcohol, hydrazine, acetone, AOT (dioctylsulfosuccinate sodium salt) obtained from POCH S.A. (Poland) were used without further purification. F12 medium, streptomycin and penicillin, glutamine, and heat-inactivated fetal bovine serum (FBS Hi) were purchased from Gibco® Life Technologies. Microbiological media (tryptic soy broth (TSB) and tryptic soy agar (TSA)) were purchased from DB. WST-8 reagent [2-(2-methoxy-4-nitrophenyl)-3-(4-nitrophenyl)-5-(2,4-disulfophenyl)-2H-tetrazolium, monosodium salt] was obtained from Sigma.

XRD details and HAADF images

For sample type Au/TiO$_2$, we observed that the peak originating from Au (2θ=38.2, 44.4, 65.1°) increased with increasing amount of Au in the samples (**Fig. 1**) [76]. We did not observe peaks related to the presence of Pd in the Pd/TiO$_2$ powders. A broad peak in the diffractograms of the bimetallic Au/Pd samples was centered intermediate between the peaks of metallic Au (2θ=38.2, 44.4°) and metallic palladium (2θ=40.1, 46.7°) (**Fig. 2**). High-angle annular dark-field (HAADF) imaging is a method of mapping samples in a scanning transmission electron microscope (STEM). These images are formed by collecting scattered electrons with an annular dark-field detector. Detector HAADF is very sensitive to differences of the element irradiated based on the atomic number (Z-contrast). In Figure 1, 2 we presented HAADF images with z-contrast combined with mapping images of monometallic Au and Pd nanoparticles deposited onto TiO$_2$. The imagesobtained by HAADF are those large (black and white). In the corner of the image provided mapping for selected samples.

Table S1. The photoactivity of monometallic and bimetallic nanoparticles deposited on TiO$_2$ calcined at 400°C in toluene and phenol degradation.

| Sample label	Amount of noble metal precursor [mol.%]		Phenol degradation after 1 h irradiation under [%]		Toluene degradation after 30 min. irradiation (mix LEDs) [%]	
	Pd	Au	Vis	UV-Vis	1st	2nd
Pure TiO$_2$	0	0	1.01	63.6	98	99
0.1Au	0	0.1	1.6	65.9	99	99
0.25Au	0	0.25	7.1	73.6	95	98
1.25Au	0	1.25	8.8	80.3	98	98
0.1Pd	0.1	0	11.3	88.2	99	98
0.25Pd	0.25	0	19.2	98.3	99	99
0.1Pd_0.1Au	0.1	0.1	9.6	86.1	80	89
0.1Pd_0.25Au	0.1	0.25	5.9	81.9	98	89
0.1Pd_0.5Au	0.1	0.5	2.3	66.1	81	95
0.1Pd_1.25Au	0.1	1.25	1.3	80.9	41	61
0.25Pd_0.25Au	0.25	0.25	6.2	91.0	83	91
0.25Pd_0.5Au	0.25	0.5	5.9	94.3	95	91
0.25Pd_1.25Au	0.25	1.25	8.2	89.1	99	95
0.5Pd_0.1Au	0.5	0.1	1.7	89.7	52	16
0.5Pd_0.25Au	0.5	0.25	10.7	92.9	94	89
0.5Pd_0.5Au	0.5	0.5	13.4	92.7	67	76
0.5Pd_1.25Au	0.5	1.25	6.6	78.9	91	88
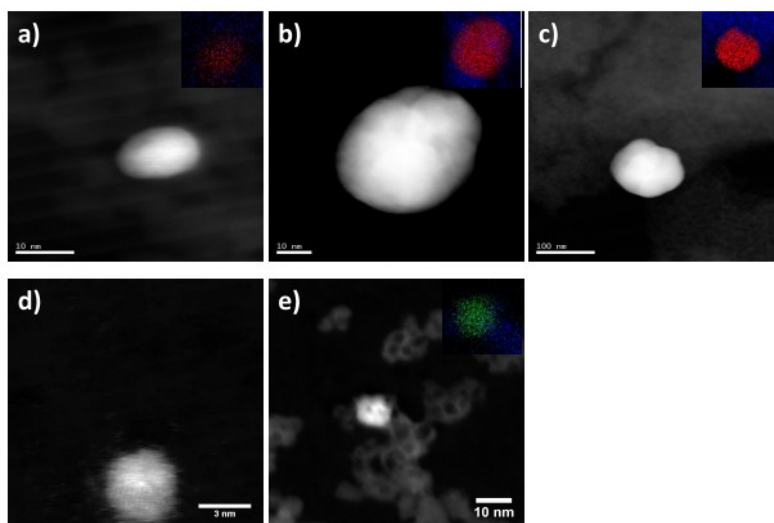
Figure S1. HAADF (high-angle annular dark-field) images with z-contrast (black and white) combined with mapping images of monometallic Au and Pd nanoparticles deposited onto TiO_2 with different metal concentrations: a) 0.1Au, b) 0.25Au, c) 1.25Au, d) 0.1Pd, e) 0.25Pd (blue is Ti, red is Au and green is Pd).
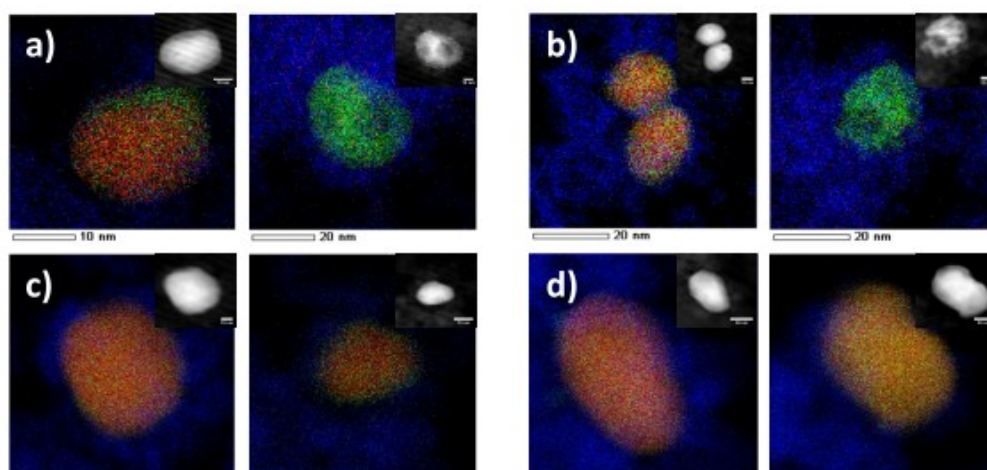

Figure S2. HAADF images with z-contrast combined with mapping images of 0.5Pd_1.25Au nanoparticles deposited onto $TiO_2$and calcined at different temperatures: (a) 350, (b) 400, (c) 450, and (d) 600°C (blue is Ti, red is Au and green is Pd).

S2. Phenol degradation under mix-LED's light

In addition we have compared the photocatalytic activity in visible light with UV-Vis and mix-LED's light. Experimental results presented in our study indicate that the average efficiency of phenol and toluene degradation under UV-Vis irradiation and mix-LED's is much higher than in case of phenol degradation under visible light (Table S1). Thus, there is no need to optimize a UV-induced and mix-LED's photocatalytic activity, as it ranges insignificantly. At the same time a deep understanding of correlation between structural features of selected second generation NPs and visible light photoactivity is still required.
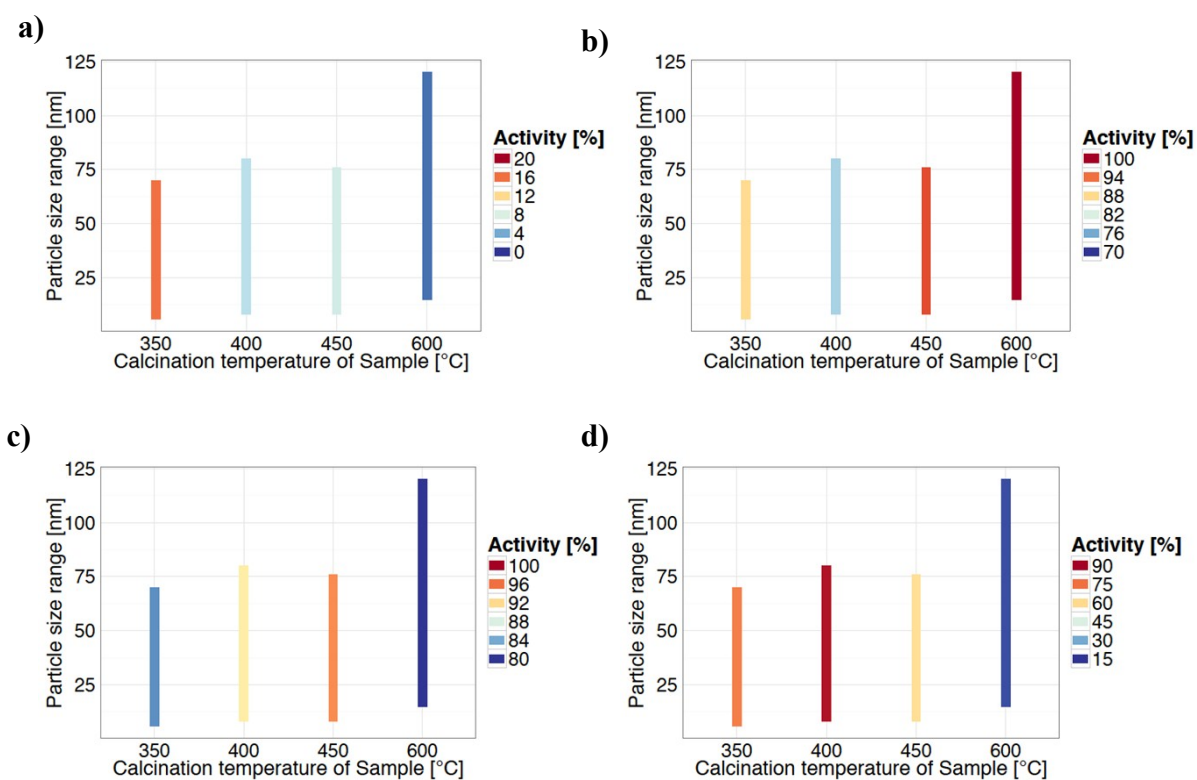
a)

b)

c)

d)

Figure S3. The influence of particle size range on the photoactivity of 0.5Pd_1.25Au calcined at different temperatures (350, 400, 450 and 600°C); the photoactivity toward phenol degradation was evaluated after 1 h of irradiation under a) visible ($\lambda > 420$ nm) and b) UV–vis light and toward toluene degradation after 0.5 h in the c) 1st and d) 2nd cycle of irradiation by mixed LEDs (5 LEDs with $\lambda_{max} = 375$ nm and 20 LEDs with $\lambda_{max} = 415$ nm).
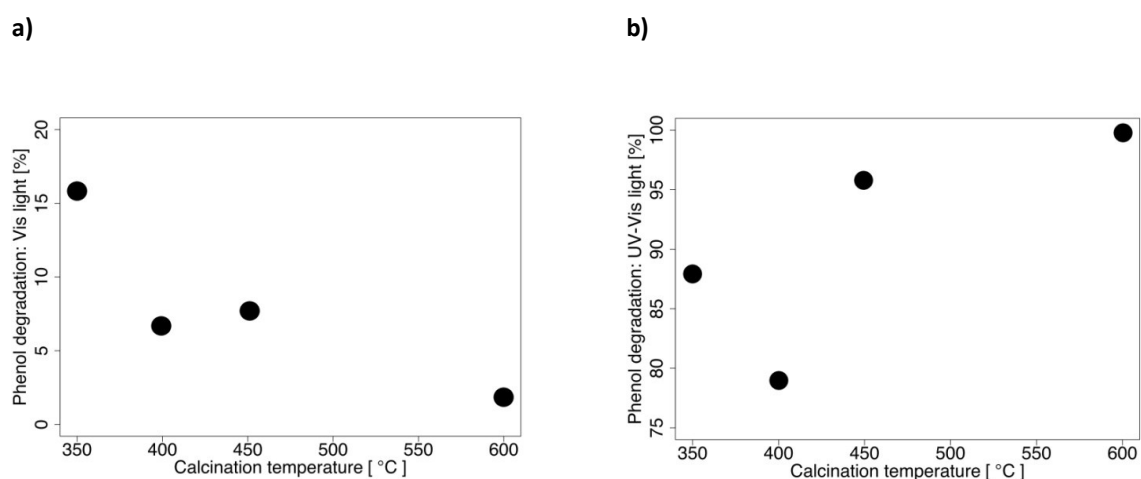
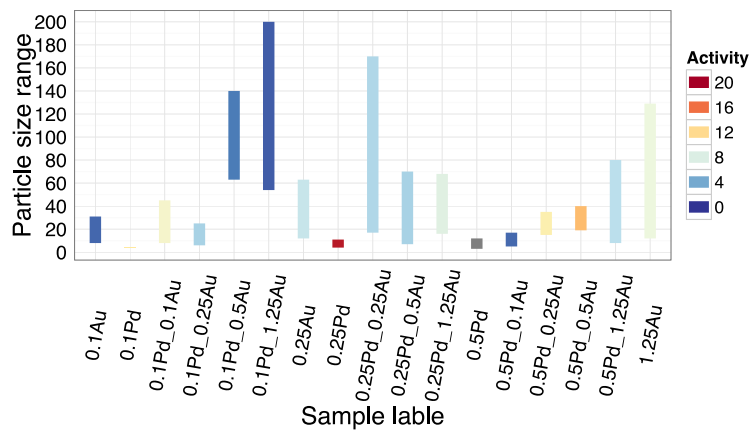a)

b)

Figure S4. The effect of calcination temperature on the photoactivity of sample obtained by using 0.5 mol.% of Pd and 1.25 mol.% of Au under a) visible ($\lambda > 420$ nm), b) UV-Vis light irradiation.
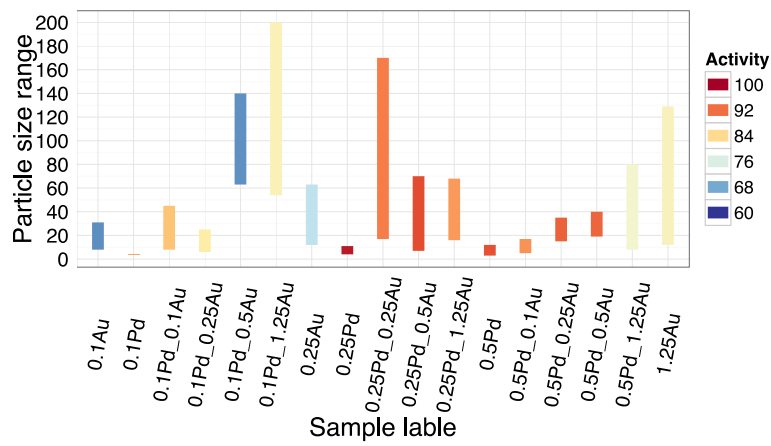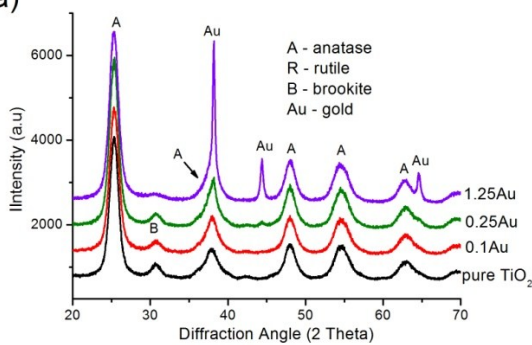
a)

b)

Figure S5. Correlation between the nanoparticle size ranges and their photocatalytic activity in phenol degradation under a) visible and b) UV–vis irradiation.

a)

b)
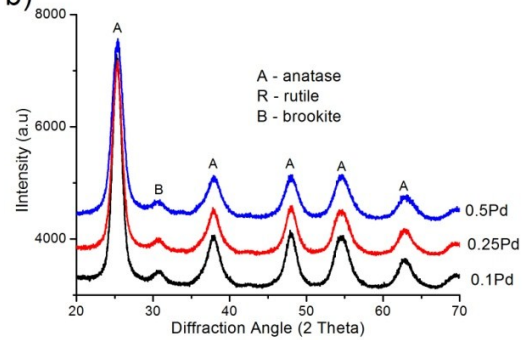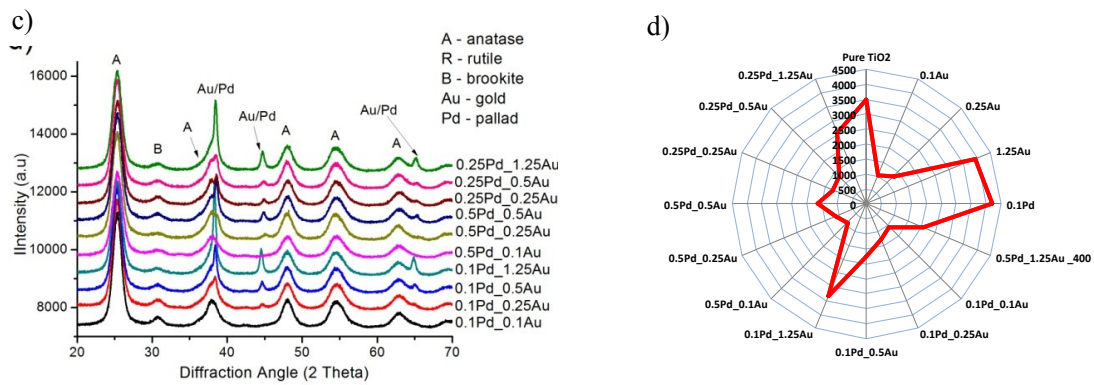
Figure S6. XRD pattern of samples: a) Au/TiO$_2$ and pure TiO$_2$, b) Pd/TiO$_2$, c) Pd_Au/TiO$_2$ with different amount of gold and palladium, d) star diagrams representing the distribution (variance) of XRD$_{anatase}$ descriptor values.

Figure S7. a) The influence of the amount of Au precursor on the BNPs structure and photocatalytic activity in phenol degradation under the influence of visible-light irradiation (λ>420 nm); b) the correlation of the BNP structure with photocatalytic activity toward phenol degradation under UV–vis and vis irradiation.

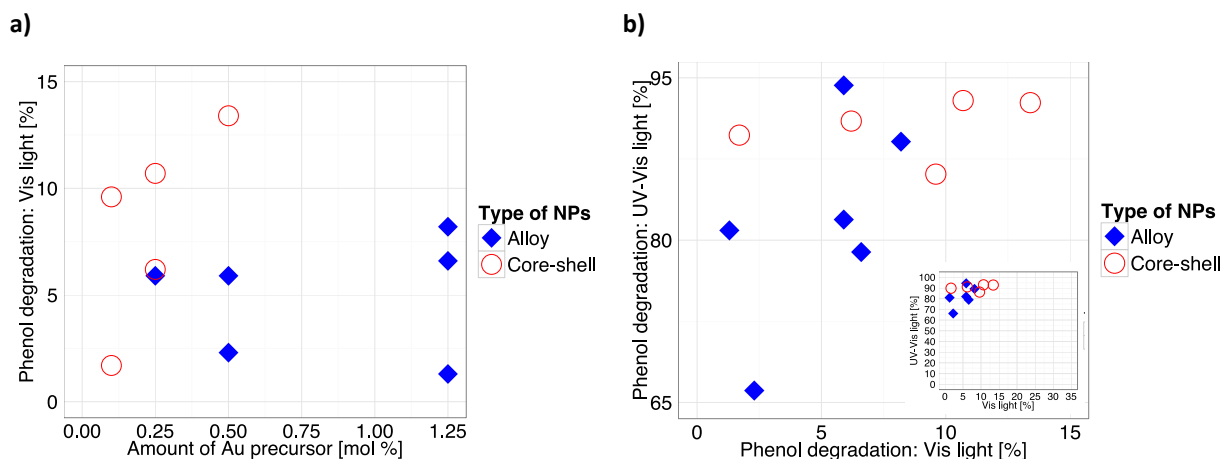**Table S2.** Summary data (descriptors) implemented in GA, towards the development of nano-QSPR model (part I).

Sample	Amount of Pd precursor [mol %]	Amount of Au precursor [mol %]	BET surface area [m²/g]	Max peak from DRS spectra [nm]	$Size_{min}$ of NPs [nm]	$Size_{max}$ of NPs [nm]	Molecular weight [g/mol]	$2\theta\ max_{Metallic\_Au}$ [°]	$2\theta\ min_{Metallic\_Au}$ [°]	$2\theta\ max_{Brukit}$ [°]	2θ max Anatase [°]	2θ min Anatase [°]	XRD_{Au} [a.u]	XRD_{Brukit} [a.u]	$XRD_{Anatase}$ [a.u]
Pure TiO$_2$	0	0	154	0	0	0	26.622			30.64	63.04	25.34		501.1	3483.3
0.1Au	0	0.1	168	572	8	31	19.697	64.54	38.02	30.9	63.18	25.32	1015.3	440.1	3581.5
0.25Au	0	0.25	139	574	12	63	49.2425	64.54	38.2	30.68	62.98	25.4	1320.5	486.1	4155.8
1.25Au	0	1.25	140	572	12	129	246.2125	64.56	38.2	30.82	63	25.38	3938.2	347	4163.8
0.1Pd	0.1	0	154	428	4	4.5	10.642			30.48	62.84	25.35		439.1	4204.9
0.25Pd	0.25	0	182	432	432	7.5	62.8	25.36	432	30.76	62.8	25.36	3582.6	418.1	4582.6
0.5Pd_1.25Au	0.5	1.25	139	614	8	45	299.4225	65.38	38.6	30.74	63	25.36	2041.2	503.1	3240.9
0.1Pd_0.1Au	0.1	0.1	156	536	6	25	30.339	44.92	37.84	30.74	63.04	25.44	1079.3	504.1	4112.7
0.1Pd_0.25Au	0.1	0.25	157	590	63	140	59.8845	65.1	38.4	30.6	62.92	25.18	1282.5	502.1	3963.3
0.1Pd_0.5Au	0.1	0.5	148	684	54	200	109.127	5.04	38.4	30.7	62.76	25.3	1764.9	434.1	3684.8
0.1Pd_1.25Au	0.1	1.25	179	614	5	17	256.8545	64.92	38.32	30.62	62.78	25.28	3328.1	381	3328.1
0.5Pd_0.1Au	0.5	0.1	136	438	15	35	72.907	38.14	38.14	30.56	62.68	25.28	899.2	421.1	3116.7
0.5Pd_0.25Au	0.5	0.25	164	462	19	40	102.4525	44.98	37.94	30.78	62.9	25.38	1117.4	1117.4	3879.2
0.5Pd_0.5Au	0.5	0.5	153	504	8	80	151.695	65.28	38.6	30.64	62.92	25.4	1633.8	487.1	3935.3
0.25Pd_0.25Au	0.25	0.25	159	548	17	170	75.8475	65.16	38.52	31.04	62.98	25.4	1218.4	456.1	3762.9
0.25Pd_0.5Au	0.25	0.5	158	590	7	70	125.09	65.3	38.54	30.74	62.78	25.4	1284.5	418.1	3887.2
0.25Pd_1.25Au	0.25	1.25	145	616	16	68	272.8175	65.18	38.42	30.52	62.92	25.36	2572.8	406.1	3596.6

Table S3. Summary data (descriptors) implemented in GA, towards the development of nano-QSPR model (part II).

| Sample	Minimal size	Maximal size	Average size	Avarage Wigner-Seits radius	number of elementary particles			ratio of surface molecules			surface-to-volume ratio		
	[nm]	[nm]	[nm]	[nm]	min	max	avarage	min	max	avarage	min	max	avarage
0.1Au	8	31	19.5	1.345902	210.00	12219.25	3041.33	0.105983	0.02735	0.04348	0.118547	0.02812	0.045457
0.25Au	12	63	37.5	1.345902	708.76	102560.7	21629.84	0.070655	0.013458	0.02261	0.076027	0.013642	0.023133
1.25Au	12	129	70.5	1.345902	708.76	880498.5	143723.2	0.070655	0.006573	0.012026	0.076027	0.006616	0.012173
0.1Pd	4	4.5	4.25	1.281871	30.384	43.26	36.44465	0.201882	0.179451	0.190007	0.252948	0.218696	0.234578
0.25Pd	11	11	11	1.281871	631.89	631.89	631.89	0.073412	0.073412	0.073412	0.079228	0.079228	0.079228
0.1Pd_0.1Au	4	45	24.5	1.313887	28.216	40175.74	6483.725	0.206924	0.018393	0.033784	0.260913	0.018738	0.034965
0.1Pd_0.25Au	6	25	15.5	1.313887	95.231	6888.84	1641.80	0.137949	0.033108	0.0534	0.160025	0.034242	0.056412
0.1Pd_0.5Au	63	140	101.5	1.313887	110242.20	1209791	461025	0.013138	0.005912	0.008155	0.013313	0.005947	0.008222
0.1Pd_1.25Au	54	200	127	1.313887	69423.67	3527088	903103.4	0.015328	0.004138	0.006517	0.015566	0.004156	0.00656
0.25Pd_0.25Au	17	170	93.5	1.313887	2166.07	2166073	360380.4	0.048688	0.004869	0.008852	0.05118	0.004893	0.008931
0.25Pd_0.5Au	7	70	38.5	1.313887	151.22	151223.9	25159.88	0.118242	0.011824	0.021499	0.134099	0.011966	0.021971
0.25Pd_1.25Au	16	68	42	1.313887	1805.87	138628.7	32664.36	0.051731	0.012172	0.019707	0.054553	0.012322	0.020103
0.5Pd_0.1Au	5	17	11	1.313887	55.110	2166.073	586.819	0.165539	0.048688	0.075245	0.198379	0.05118	0.081368
0.5Pd_0.25Au	15	35	25	1.313887	1487.99	18902.99	6888.84	0.05518	0.023648	0.033108	0.058402	0.024221	0.034242
0.5Pd_0.5Au	19	40	29.5	1.313887	3024.04	28216.7	11318.59	0.043563	0.020692	0.028058	0.045547	0.02113	0.028867

Table S4. Statistic parameters towards development of Nano-QSPR model.

No	Name	Suitableto	Coefficient		Description ofCoefficient
1	**The normalization process**	**Z-scores**	$z_i = \dfrac{x_i - \bar{x}_j}{s_j}$		where: z_i is the transformed value of a given variable, x_i - is the original value of a given variable, $\bar{x}_j$ is the mean value of a given variable calculated across a group of trening set compounds, s_j the standard deviation of a given variable calculated across a group of trening set compounds.
2	The correlation coefficient The root mean square error of calibration	Measure of goodness-of-fit	$R^2 = 1 - \dfrac{\sum_{i=1}^{n}(y_i^{obs} - y_i^{pred})^2}{\sum_{i=1}^{n}(y_i^{obs} - \tilde{y}^{obs})^2}$	$RMSEC = \sqrt{\dfrac{\sum_{i=1}^{n}(y_i^{obs} - y_i^{pred})^2}{n}}$	where: y_j^{obs} – experimental (observed) value of the property for the ith compound from the training set; y_i^{pred} – predicted value for i^{th} compound from the training set; y^{obs} – the mean experimental value of the property in the training set; n – the number of compounds in the training set.
3	The cross-validated coefficient The root mean square error of calibration	Measure stability of the model	$Q_{LOO}^2 = 1 - \dfrac{\sum_{i=1}^{n}(y_i^{obs} - y_i^{predcv})^2}{\sum_{i=1}^{n}(y_i^{obs} - \tilde{y}^{obs})^2}$	$RMSECV = \sqrt{\dfrac{\sum_{i=1}^{n}(y_i^{obs} - y_i^{predcv})^2}{n}}$	where: y_j^{obs} – experimental (observed) value of the property for the ith compound; y_i^{predcv} – cross-validated predicted valuef or i^{th} compound; y – the mean experimental value of the property in the training set; n – the number of compounds in the training set.
4	The external-validation coefficient The root mean square error of prediction	Measure external predictivity	$Q_{EXT}^2 = 1 - \dfrac{\sum_{j=1}^{k}\left(y_j^{obs} - y_j^{pred}\right)^2}{\sum_{j=1}^{k}\left(y_j^{obs} - \hat{y}^{obs}\right)^2}$	$RMSEP = \sqrt{\dfrac{\sum_{j=1}^{k}\left(y_j^{obs} - y_j^{pred}\right)^2}{k}}$	where: y_j^{obs} – experimental (observed) value of the property for the jth compound from the validation set; y_j^{pred} – predicted valuef or j^{th} compound from the validation set; $\hat{y}^{obs}$ – the mean experimental value of the property in the validation set; k – the number of compounds in the validation set. Squared correlation coefficient values between the observed and predicted values of the compounds with/without intercept (r^2 / r_0^2).
		Mean absolute error		$MEA = \dfrac{1}{k}\sum y_j^{obs} - y_j^{pred}$	

		The accuracy and different variants of r^2_m	$$r_m^2 = r^2 \left(1 - \sqrt{r^2 - r_0^2}\right)$$
5	Concordance Correlation Coefficient	Restrictive parameter for expressing external predictivity	$$CCC = \frac{2\sum_{j=1}^{k_{EXT}} \left(y_j^{obs} - \hat{\bar{y}}^{obs}\right)\left(y_j^{pred} - \hat{\bar{y}}^{pred}\right)}{\sum_{j=1}^{k_{EXT}}\left(y_j^{obs} - \hat{\bar{y}}^{obs}\right)^2 + \sum_{j=1}^{k_{EXT}}\left(y_j^{pred} - \hat{\bar{y}}^{pred}\right)^2 + k_{EXT}\left(\hat{\bar{y}}^{obs} - \hat{\bar{y}}^{pred}\right)^2}$$

Table S5. Applicability domain based on the standardization approach.

Sample Name	Descriptor $XRD_{anatase}$	Descriptor $Pd_{\%mol}$	Outlier Info.	Split
Pure TiO$_2$	3483.3	0	-	Training set
0.1Pd_1.25Au	3328.1	0.1	-	Training set
0.1Au	3116.7	0.5	-	Training set
0.5Pd_0.1Au	3684.8	0.1	-	Training set
0.1Pd_0.5Au	3887.2	0.25	-	Training set
0.1Pd_0.25Au	3762.9	0.25	-	Training set
0.25Pd_0.5Au	4155.8	0	-	Training set
0.25Pd_0.25Au	3596.6	0.25	-	Training set
0.5Pd_1.25Au	4112.7	0.1	-	Training set
0.25Au	3879.2	0.5	-	Training set
0.25Pd_1.25Au	3935.3	0.5	-	Training set
1.25Au	4582.6	0.25	-	Training set
0.1Pd_0.1Au	3581.5	0		Validation set
0.5Pd_0.25Au	3963.3	0.1	-	Validation set
0.1Pd	3240.9	0.5	-	Validation set
0.5Pd_0.5Au	4163.8	0	-	Validation set
0.25Pd	4204.9	0.1	-	Validation set
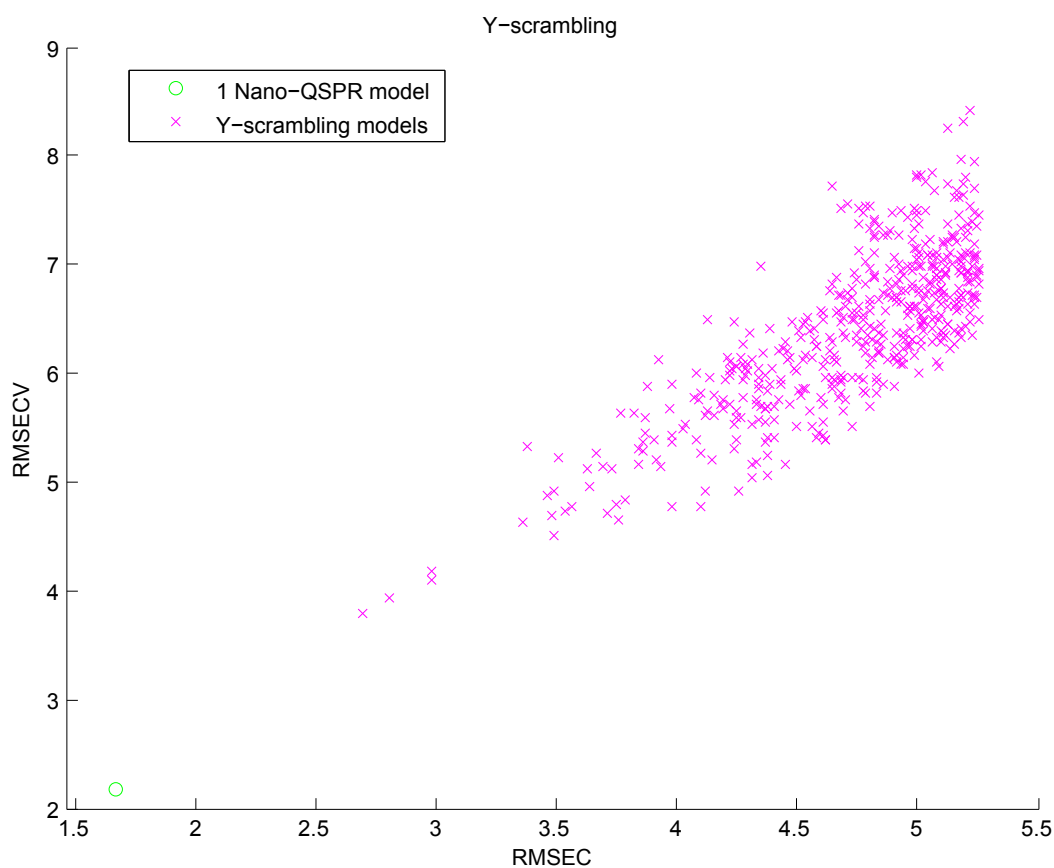
Figure S8. The results of the Y-scrambling test (green circle is the original model).